

Coulomb corrections in rare decays of neutral B mesons with $\ell^+\ell^-$ -pair in final state

S.I. Manukhov^{*1,2} and N.V. Nikitin^{1,2,3}

¹*Faculty of Physics, Lomonosov Moscow State University, Russia, Moscow, 119234*

²*Skobeltsyn Institute of Nuclear Physics, Lomonosov Moscow State University, Russia, Moscow, 119234*

³*Moscow Institute of Physics and Technology, Russia, Moscow, 141701*

(Dated: February 10, 2026)

We present a systematic analysis of Coulomb corrections for leptonic ($B_{d,s}^0 \rightarrow \ell^+\ell^-$), semileptonic ($B_{d,s}^0 \rightarrow h^0\ell^+\ell^-$, $B_{d,s}^0 \rightarrow V^0\ell^+\ell^-$) and radiative leptonic ($B_{d,s}^0 \rightarrow \gamma\ell^+\ell^-$) decays of neutral B -mesons. The relativization of the Coulomb factor was performed by comparing the Gamow-Sommerfeld-Sakharov factor, the exact relativistic approach of Crater-Alstine-Sazdjian applied by us to scalar systems, and well-known one-loop QED calculations. Coulomb corrections are calculated for differential, angular, and double-differential distributions, as well as for partial decay widths.

For the $B_s^0 \rightarrow \mu^+\mu^-$ channel, Coulomb corrections improve the prediction of the partial width to $\delta = |\mathcal{B}^{(exp)} - \mathcal{B}^{(theory)}|/\mathcal{B}^{(exp)} = 2\%$. This improvement brings the prediction closer to the LHCb/CMS experimental results within the current experimental (11%) and theoretical (5% lattice QCD) errors. In the decays $B^0 \rightarrow K^0\mu^+\mu^-$ and $B^0 \rightarrow K^{0*}\mu^+\mu^-$, Coulomb effects also reduce the discrepancies between theoretical predictions and experimental data (to less than $\delta = 1\%$ and from $\delta = 11\%$ to $\delta = 4\%$ respectively). Finally, for the decays involving τ -leptons, the Coulomb correction $\mathcal{K} = \mathcal{B}^{(Coulomb)}/\mathcal{B}^{(free)}$ reaches 4%. While currently smaller than the dominant form-factor uncertainties and experimental errors, the Coulomb correction represents a non-negligible systematic effect. It should be accounted for in the high-precision era of B -physics, where such effects may become significant for the interpretation of potential New Physics signals.

PACS numbers: 13.20.He; 13.25.-k; 14.40.Nd

I. INTRODUCTION

Rare semileptonic and ultra-rare leptonic decays of B mesons are under intensive investigation at the LHCb [1–10], CMS [11–13], and ATLAS [14] experiments at the Large Hadron Collider, as well as in the Belle-II experiment [15–17]. At the current moment the partial widths of the leptonic decays $B_{d,s}^0 \rightarrow \mu^+\mu^-$ have been measured [6, 13, 14], along with the semileptonic decays $B_{d,s}^0 \rightarrow X^0\ell^+\ell^-$ (where $X^0 = K^{0(*)}, \eta, \phi, \omega, \pi^0, \rho^0, \dots$ is a pseudoscalar or vector meson) [1, 15]. Upper limits have also been established for the leptonic radiative decay $B_s^0 \rightarrow \gamma\ell^+\ell^-$ [2]. Differential and angular distributions have been obtained for the decays $B^0 \rightarrow K^{0(*)}\mu^+\mu^-$ and $B_s^0 \rightarrow \phi\mu^+\mu^-$ [1, 8–11].

These decays have been theoretically studied in detail both within the Standard Model (SM) and in its extensions. Some works on this broad topic can be found in Refs. [18–24]. The persistent discrepancies between experimental results and theoretical predictions motivate further refinement of theoretical calculations. A typical example of such discrepancy is the partial width of the $B_s^0 \rightarrow \mu^+\mu^-$ decay, measured by the ATLAS [14], CMS [13], and LHCb [5, 7]. While measurements before 2022 were systematically lower than the SM predictions [21], the latest data from CMS [13] show a central value slightly exceeding theoretical expectations.

More noticeable deviations are observed in the differen-

tial distributions of $B^0 \rightarrow K^0\mu^+\mu^-$ [9], $B^0 \rightarrow K^{0*}\mu^+\mu^-$ [1, 8], and $B_s^0 \rightarrow \phi\mu^+\mu^-$ [10]. In the region of low transferred momentum squared $q^2 = (p_B - p_X)^2$, the Standard Model predictions systematically exceed the experimental data.

The aim of this paper is to account for the Coulomb interaction between charged leptons in the final state in decays of neutral B mesons. In Section II, several approaches for calculating Coulomb corrections are compared: the non-relativistic Gamow-Sommerfeld-Sakharov (GSS) method, the relativistic Crater-Alstine-Sazdjian (CAS) formalism based on exact two-particle relativistic equations, and the approach based on loop calculations in QED. In Section III, the Coulomb correction is applied for the analysis of ultra-rare leptonic decays $B_{d,s}^0 \rightarrow \ell^+\ell^-$; in Section IV, for the analysis of rare semileptonic decays $B_{d,s}^0 \rightarrow h^0\ell^+\ell^-$ with a pseudoscalar meson h^0 ; in Section V, for the analysis of rare semileptonic decays $B_{d,s}^0 \rightarrow V^0\ell^+\ell^-$ with a vector meson V^0 ; and in Section VI, for the analysis of rare radiative semileptonic decays $B_{d,s}^0 \rightarrow \gamma\ell^+\ell^-$.

II. COMPARISON OF METHODS FOR COULOMB CORRECTION CALCULATION

The Coulomb interaction is described by the \mathcal{K} -factor:

$$\mathcal{K} = \frac{\Gamma^{(Coulomb)}}{\Gamma^{(free)}}, \quad (1)$$

*Email: manuhov2000akk@gmail.com

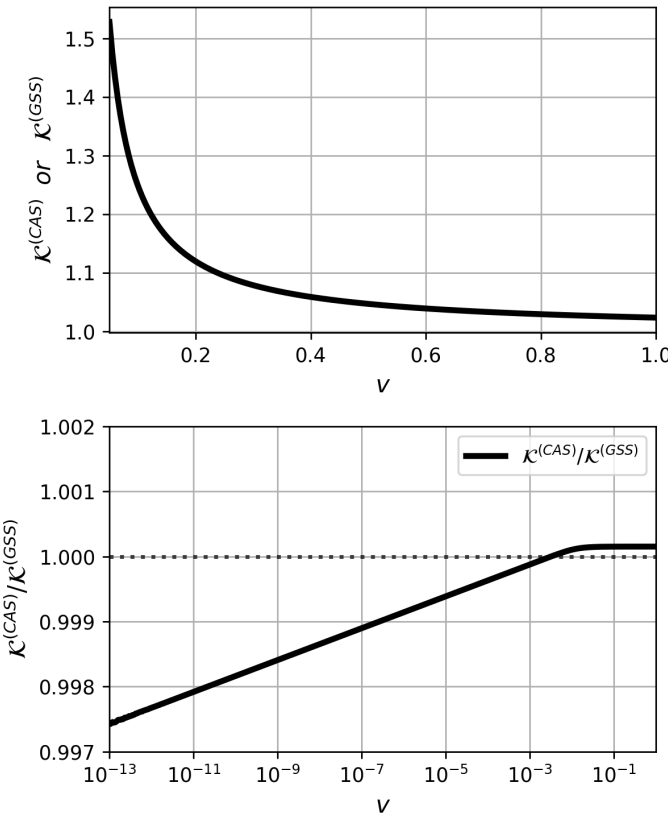


FIG. 1: The dependence of the Coulomb \mathcal{K} -factor as a function of the relative velocity $v = v_{rel}$ (top), and the ratio $\mathcal{K}^{(CAS)}/\mathcal{K}^{(GSS)}$ of the factors as a function of v (bottom). The smaller the velocity, the larger the Coulomb enhancement. It can be seen that the *CAS* and *GSS* methods yield practically identical results over the entire range of significant velocities $v \in [10^{-15}, 1]$. The relative difference across considered range of velocities does not exceed 0.3%.

where $\Gamma^{(\text{Coulomb})}$ denotes the decay width with the Coulomb interaction in the final state, and $\Gamma^{(\text{free})}$ denotes the width without such interaction.

The \mathcal{K} -factor can be calculated using several methods. To validate the approach for neutral B -meson decays, we first benchmark these methods against a simpler process: the decay of a hypothetical neutral scalar particle $B^0(M)$ into two hypothetical charged scalars $S^+(m)$ and $S^-(m)$. In Subsection II A, we discuss the approach of Gamow, Sommerfeld, and Sakharov, while in Subsection II B, we apply the method developed by Crater, Alstine, and Sazdjian for this decay. In the Subsection II C, in which we discuss the one-loop calculations, the Coulomb correction for particles with non-zero spin is also addressed.

A. Gamow-Sommerfeld-Sakharov (GSS) Method

The Gamow–Sommerfeld–Sakharov coefficient [25–27] accounts for the Coulomb interaction at *non-relativistic* velocities. This correction, obtained from the Schrödinger equation for the relative motion, takes the form:

$$\mathcal{K}^{(GSS)}(v) = \frac{2\pi\alpha_{\text{em}}/v}{1 - e^{-2\pi\alpha_{\text{em}}/v}}, \quad (2)$$

where $v = v_{rel}$ is the relative velocity of particles S^+ and S^- , and $\alpha_{\text{em}} \approx 1/137$ is the fine structure constant.

B. Crater-Alstine-Sazdjian (CAS) Formalism

The Crater-Alstine-Sazdjian formalism [28–30] is a method based on constructing exact relativistic two-particle equations. This approach utilizes classical relativistic dynamics with constraints followed by quantization. A brief overview of the CAS approach using the example of scalar particles is provided in Appendix A. Applying this formalism to the scalar decay leads to the following Coulomb correction (proof is given in Appendix B):

$$\mathcal{K}^{(CAS)}(v) = \left| \frac{\Gamma\left(\sqrt{\frac{1}{4} - \alpha_{\text{em}}^2} + \frac{1}{2} + i\frac{\alpha_{\text{em}}}{v}\right)}{\Gamma\left(\sqrt{1 - 4\alpha_{\text{em}}^2} + 1\right)} \right|^2 \cdot e^{\pi\alpha_{\text{em}}/v}, \quad (3)$$

where $\Gamma(x)$ is Euler's gamma function.

The dependence of the \mathcal{K} -factor on the relative velocity v of the S^+S^- pair is shown in Fig. 1, top. It can be seen that the smaller the final relative velocity, the larger the magnitude of the Coulomb correction. The *CAS* and *GSS* corrections yield practically identical results over the entire physically significant velocity range. The ratio of these factors is shown in Fig. 1, bottom.

The numerical difference between the *CAS* and *GSS* corrections does not exceed 0.3% in the non-relativistic limit ($v = 10^{-15}$):

$$\left. \frac{\mathcal{K}^{(CAS)}}{\mathcal{K}^{(GSS)}} \right|_{v=10^{-15}} \approx 0.997. \quad (4)$$

In the relativistic regime ($v \approx 1$), the discrepancy between the methods becomes smaller:

$$\lim_{v \rightarrow 1} \frac{\mathcal{K}^{(CAS)}}{\mathcal{K}^{(GSS)}} \approx 1.0002. \quad (5)$$

C. Loop QED Approach

In quantum field theory, the Coulomb correction naturally emerges from one-loop QED calculations. As shown

in [31], the one-loop correction to charged particle annihilation contains a Coulomb singularity matching the GSS

factor expansion:

$$\Gamma^{1\text{-loop}} \Big|_{s \rightarrow 4m^2} = \Gamma^{\text{Born}} \left[1 + \pi \alpha_{\text{em}} \frac{s - 2m^2}{\sqrt{s(s - 4m^2)}} + O\left(\sqrt{1 - \frac{4m^2}{s}}\right) \right], \quad (6)$$

where s is the Mandelstam variable, and Γ^{Born} is the Born decay width. This corresponds to $\mathcal{K} \approx 1 + \pi \alpha_{\text{em}} / v_{\text{rel}} + O(\alpha_{\text{em}} / v_{\text{rel}})$. Replacing the non-relativistic relative velocity with its relativistic counterpart v_{rel} thus ensures consistency with QED. Moreover, the universal part of this final-state QED correction is spin-independent, justifying its application to decays involving leptons.

Based on the analysis performed, we conclude that both factor (2) or (3) can be applied to decays of neutral B -mesons. Indeed, the discrepancy between the two factors does not exceed 0.3%, which is significantly smaller than $\sim 5\text{-}10\%$ [13, 32] of the current experimental errors and the theoretical uncertainties corresponding to non-

perturbative contributions to hadronic form-factors.

III. COULOMB INTERACTION IN $B_{d,s}^0 \rightarrow \ell^+ \ell^-$ DECAYS

In this section we consider the decay of a neutral B -meson (P, M) into a lepton pair $\ell^+(p_1, m_\ell) \ell^-(p_2, m_\ell)$ accounting for the Coulomb interaction in the final state.

Neglecting the masses of the light quarks q , the effective Hamiltonian for $b \rightarrow q \ell^+ \ell^-$ transitions ($q = d, s$) is written as a Wilson operator product expansion [19, 33]:

$$\mathcal{H}_{\text{eff}}^{b \rightarrow q \ell^+ \ell^-}(x) = \frac{G_F}{\sqrt{2}} \frac{\alpha_{\text{em}}}{2\pi} V_{tb} V_{tq}^* \left[-2im_b \frac{C_7(\mu)}{q^2} \cdot \bar{q}(x) \sigma_{\mu\nu} q^\nu (1 + \gamma_5) b(x) \cdot \bar{\ell}(x) \gamma^\mu \ell(x) \right. \\ \left. + C_{9V}(\mu) \cdot \bar{q}(x) \gamma_\mu (1 - \gamma_5) b(x) \cdot \bar{\ell}(x) \gamma^\mu \ell(x) + C_{10A}(\mu) \cdot \bar{q}(x) \gamma_\mu (1 - \gamma_5) b(x) \cdot \bar{\ell}(x) \gamma^\mu \gamma_5 \ell(x) \right] + h.c., \quad (7)$$

where G_F is the Fermi constant, V_{tb} and V_{tq} are elements of the Cabibbo-Kobayashi-Maskawa matrix [34], q^ν is the 4-momentum of the lepton pair, and $q^2 = q^\nu q_\nu$. Here, $\sigma^{\mu\nu} = \frac{i}{2} [\gamma^\mu, \gamma^\nu]$, $\gamma^5 = i \gamma^0 \gamma^1 \gamma^2 \gamma^3$, and $\varepsilon^{0123} = -1$. The scale parameter $\mu \sim m_b \sim 5$ GeV separates perturbative and non-perturbative contributions of the strong interaction. The perturbative contribution is contained in the Wilson coefficients $C_7(\mu)$, $C_{9V}(\mu)$, and $C_{10A}(\mu)$. The non-perturbative contribution arises mainly in the computation of the matrix elements of the Hamiltonian (7) between the initial and final hadronic states.

Within the SM, at $\mu_0 = 5$ GeV, the following numerical values for the Wilson coefficients can be obtained: $C_1(\mu_0) = 0.241$, $C_2(\mu_0) = -1.1$, $C_3(\mu_0) = -0.0104$, $C_4(\mu_0) = 0.02433$, $C_5(\mu_0) = -0.00706$, $C_6(\mu_0) = 0.0294$, $C_7(\mu_0) = 0.312$, $C_{9V}(\mu_0) = -4.21$, and $C_{10A}(\mu_0) = 4.41$ [19, 33, 35].

The matrix element of the axial current is determined via the decay constant $f_{B_q^0}$ [32]:

$$\langle 0 | \bar{q}(0) \gamma^\mu \gamma^5 b(0) | B_{d,s}^0(M, P) \rangle = i f_{B_{d,s}^0} P^\mu. \quad (8)$$

Application of the Coulomb correction in the form of the CAS \mathcal{K} -factor for the leptonic decay yields the following value for the partial decay width of $B_{d,s}^0 \rightarrow \ell^+ \ell^-$:

$$\Gamma_{B_{d,s}^0 \rightarrow \ell^+ \ell^-}^{(\text{Coulomb})} = \Gamma_{B_{d,s}^0 \rightarrow \ell^+ \ell^-}^{(\text{free})} \cdot \mathcal{K}^{(\text{CAS})}(v) \quad (9)$$

where $\Gamma_{B_{d,s}^0 \rightarrow \ell^+ \ell^-}^{(\text{free})}$ is the decay width without accounting for the Coulomb interaction, the exact formula for which is given in [21]. The argument v , which we substitute into the correction factor $\mathcal{K}^{(\text{CAS})}(v)$, is equal to:

$$v = \frac{\sqrt{1 - 4(m_\ell/M_B)^2}}{1 - 2(m_\ell/M_B)^2},$$

and represents the relative velocity of the $\ell^+ \ell^-$ pair.

A comparison of experimental data and theoretical predictions for the decays $B_{d,s}^0 \rightarrow \ell^+ \ell^-$ is presented in Table I. As a measure of the theory-experiment discrepancy, we use the quantity:

$$\delta = \frac{|\mathcal{B}^{(\text{exp})} - \mathcal{B}^{(\text{theory})}|}{\mathcal{B}^{(\text{exp})}}, \quad (10)$$

where $\mathcal{B}^{(exp)}$ and $\mathcal{B}^{(theory)}$ are the experimental and theoretical branching fractions.

The SM predictions for the decays $B_{d,s}^0 \rightarrow \mu^+ \mu^-$ without account of the Coulomb interaction are taken from [21]. The value of the Coulomb correction for all decays is about $\mathcal{K} = 2.3\%$. It can be seen that for the decay $B_s^0 \rightarrow \mu^+ \mu^-$, accounting for the Coulomb interaction improves the agreement between the SM predictions and the experimental data: the discrepancy between the average experimental value and the corrected theoretical prediction reduces to $\delta = 2\%$. The experimental error is 11% [13], and the theoretical prediction error is about 5%, mainly due to the uncertainty in the decay constant $f_{B_{d,s}^0}$ in lattice calculations [32].

	$\mathcal{B}^{(exp)}$ [13, 34]	$\mathcal{B}^{(free)}$ [21]	$\mathcal{B}^{(Coulomb)}$
$B_s^0 \rightarrow \mu^+ \mu^- [10^{-9}]$	$3.83^{+0.44}_{-0.41}$	3.66 ± 0.14	3.75 ± 0.14
$B^0 \rightarrow \mu^+ \mu^- [10^{-11}]$	< 19 at 95% CL	1.03 ± 0.05	1.05 ± 0.05
$B_s^0 \rightarrow e^+ e^- [10^{-11}]$	< 940 at 90% CL	1.77 ± 0.08	1.81 ± 0.09
$B^0 \rightarrow e^+ e^- [10^{-13}]$	< 25000 at 90% CL	4.99 ± 0.25	5.10 ± 0.26
$B_s^0 \rightarrow \tau^+ \tau^- [10^{-8}]$	$< 6.8 \cdot 10^5$ at 90% CL	4.61 ± 0.22	4.75 ± 0.23
$B^0 \rightarrow \tau^+ \tau^- [10^{-9}]$	$< 2.1 \cdot 10^6$ at 90% CL	1.28 ± 0.07	1.32 ± 0.07

TABLE I: Partial decay widths for $B_{d,s}^0 \rightarrow \ell^+ \ell^-$. Comparison of experimental data, theoretical SM predictions without account of Coulomb interaction between particles in the final state, and predictions including this interaction.

IV. COULOMB INTERACTION IN $B_{d,s}^0 \rightarrow h^0 \ell^+ \ell^-$ DECAYS

This section applies the Coulomb correction to analyse the decays $B^0 \rightarrow h^0 \ell^+ \ell^-$, where h^0 is a neutral pseudoscalar meson. The differential decay widths are given by:

$$\frac{d\Gamma_{B_{d,s}^0 \rightarrow h^0 \ell^+ \ell^-}^{(\text{Coulomb})}}{d\hat{s}} = \frac{d\Gamma_{B_{d,s}^0 \rightarrow h^0 \ell^+ \ell^-}^{(\text{free})}}{d\hat{s}} \cdot \mathcal{K}^{(CAS)}(v), \quad (11)$$

where $\hat{s} = q^2/M_B^2 = (p_B - p_h)^2/M_B^2$, $\hat{m} = (m_\ell/M_B)^2$, and $d\Gamma_{B_{s,q}^0 \rightarrow h^0 \ell^+ \ell^-}/d\hat{s}$ is the differential width without Coulomb interaction, whose exact form is provided in the [22]. Relative velocity v is equal to:

$$v = \frac{\sqrt{1 - 4\hat{m}/\hat{s}}}{1 - 2\hat{m}/\hat{s}}.$$

Within this study, calculations were performed for the decays $B^0 \rightarrow \{K^0, \pi^0\} \ell^+ \ell^-$ and $B_s^0 \rightarrow \{\eta, \eta', K^0\} \ell^+ \ell^-$. Differential, angular, and double differential distributions

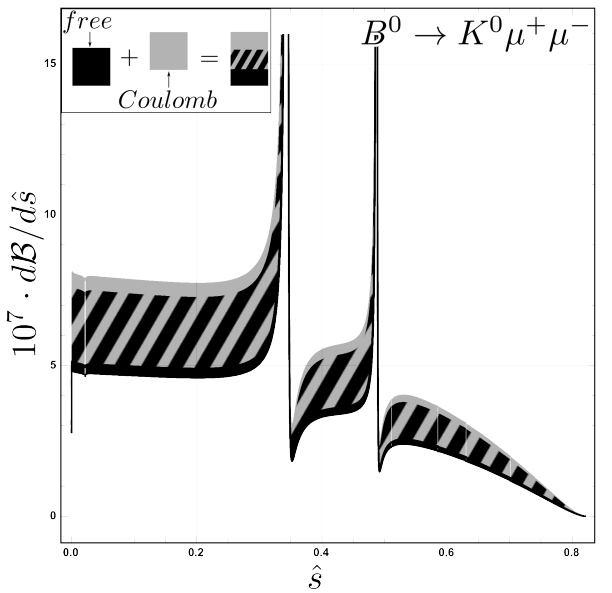


FIG. 2: Dependence of the differential branching fraction $10^7 d\mathcal{B}/d\hat{s}$ for the decay $B^0 \rightarrow K^0 \mu^+ \mu^-$ on $\hat{s} = (p_B - p_K)^2/M_B^2$ – the squared transferred momentum normalized to the square of the B -meson mass. The black band corresponds to predictions without Coulomb interaction, the gray band – with Coulomb interaction. The overlap region is indicated by black-gray hatching.

are shown in Figs. 3, 4 and 5 in Appendix C. A typical example of the differential distribution for the decay $B^0 \rightarrow K^0 \mu^+ \mu^-$ is shown in Fig. 2. The main contribution to the calculation uncertainty is associated with the error in the hadronic transition form-factors (values taken from [36, 37]). Accounting for the Coulomb interaction leads to a slight upward shift of the entire curve, remaining within the error band.

In accordance with the experimental procedure [8], when calculating the total decay width, resonant peaks for J/ψ and $\psi(2S)$ mesons are excluded in the regions:

$$q^2 \in [8, 11] \text{ GeV}^2, \text{ and } q^2 \in [12.5, 15] \text{ GeV}^2. \quad (12)$$

To estimate the contribution of non-resonant processes in the excluded regions, the value of the differential width was assumed constant and equal to the arithmetic mean of the values at the boundaries of the intervals. The values of the partial decay widths are given in Table II.

For $B^0 \rightarrow K^0 \mu^+ \mu^-$, the Coulomb corrections reduce the discrepancy between theory and experiment from $\delta = 1.7\%$ to $\delta = 0.5\%$. Given the 10% uncertainties in both experimental and theoretical predictions, this level of agreement may reflect statistical fluctuations.

For the decay $B^0 \rightarrow K^0 e^+ e^-$, the Coulomb correction formally increases the discrepancy from $\delta = 33\%$ to $\delta = 36\%$, while still remaining within the 45% experimental uncertainty.

For decays involving τ -leptons, the Coulomb correction is of the order of $\mathcal{K} \approx 4\%$. While this is currently

	$\mathcal{B}^{(exp)}$	$\mathcal{B}^{(free)}$	$\mathcal{B}^{(Coulomb)}$	\mathcal{K}
$B^0 \rightarrow K^0 e^+ e^- [10^{-7}]$	$2.5^{+1.1}_{-0.9}$	3.34 ± 0.37	3.42 ± 0.39	2.3%
$B^0 \rightarrow K^0 \mu^+ \mu^- [10^{-7}]$	3.39 ± 0.35	3.33 ± 0.38	3.41 ± 0.38	2.3%
$B^0 \rightarrow K^0 \tau^+ \tau^- [10^{-8}]$	-	5.0 ± 2.1	5.18 ± 2.2	3.3%
$B^0 \rightarrow \pi^0 e^+ e^- [10^{-8}]$	< 8.4	1.17 ± 0.3	1.19 ± 0.3	2.3%
$B^0 \rightarrow \pi^0 \mu^+ \mu^- [10^{-8}]$	< 6.9	1.16 ± 0.3	1.19 ± 0.3	2.3%
$B^0 \rightarrow \pi^0 \tau^+ \tau^- [10^{-9}]$	-	3.05 ± 0.73	3.15 ± 0.76	3.0%
$B_s^0 \rightarrow \eta e^+ e^- [10^{-7}]$	-	4.12 ± 0.79	4.22 ± 0.80	2.3%
$B_s^0 \rightarrow \eta \mu^+ \mu^- [10^{-7}]$	-	4.11 ± 0.79	4.21 ± 0.80	2.4%
$B_s^0 \rightarrow \eta \tau^+ \tau^- [10^{-8}]$	-	7.04 ± 1.2	7.28 ± 1.3	3.3%
$B_s^0 \rightarrow \eta' e^+ e^- [10^{-7}]$	-	3.04 ± 0.58	3.11 ± 0.59	2.3%
$B_s^0 \rightarrow \eta' \mu^+ \mu^- [10^{-7}]$	-	3.03 ± 0.58	3.10 ± 0.59	2.3%
$B_s^0 \rightarrow \eta' \tau^+ \tau^- [10^{-8}]$	-	2.37 ± 0.36	2.47 ± 0.38	3.9%
$B_s^0 \rightarrow K^0 e^+ e^- [10^{-8}]$	-	1.35 ± 0.34	1.38 ± 0.35	2.3%
$B_s^0 \rightarrow K^0 \mu^+ \mu^- [10^{-8}]$	-	1.34 ± 0.34	1.37 ± 0.35	2.4%
$B_s^0 \rightarrow K^0 \tau^+ \tau^- [10^{-9}]$	-	2.55 ± 0.59	2.64 ± 0.62	3.3%

TABLE II: Partial decay widths for $B^0 \rightarrow \{K^0, \pi^0\} \ell^+ \ell^-$ and $B_s^0 \rightarrow \{\eta, \eta', K^0\} \ell^+ \ell^-$. Experimental data is taken from [34].

smaller than the dominant form-factor uncertainties, it constitutes a systematic effect that must be accounted for in future high-precision experimental analyses.

V. COULOMB INTERACTION IN $B_{d,s}^0 \rightarrow V^0 \ell^+ \ell^-$ DECAYS

This section examines the Coulomb interaction in the decays $B^0 \rightarrow \{K^{0*}, \rho^0\} \ell^+ \ell^-$ and $B_s^0 \rightarrow \{\phi, K^{0*}\} \ell^+ \ell^-$ involving a neutral vector meson. The differential decay width is determined similarly to (11) with the pseudoscalar meson h^0 replaced by the vector meson V^0 . The explicit expression for $d\Gamma_{B_{s,d}^0 \rightarrow V^0 \ell^+ \ell^-}^{(\text{free})}/d\hat{s}$ is derived from the theoretical framework described in the [22].

Differential, angular and double differential distributions are shown on Figs. 6, 7 and 8 in Appendix C. The predicted partial widths, obtained with the procedure of cutting out the peak regions defined in (12), are presented in Table III.

An interesting feature can be observed in the angular distributions $d\mathcal{B}/d\cos\theta$, where θ is the angle between the direction of the neutral hadron h^0 and the positive lepton ℓ^+ in the $\ell^+ \ell^-$ rest frame. When comparing the

	$\mathcal{B}^{(exp)}$	$\mathcal{B}^{(free)}$	$\mathcal{B}^{(Coulomb)}$	\mathcal{K}
$B^0 \rightarrow K^{0*} e^+ e^- [10^{-6}]$	1.19 ± 0.20	1.36 ± 0.15	1.40 ± 0.15	2.4%
$B^0 \rightarrow K^{0*} \mu^+ \mu^- [10^{-6}]$	1.06 ± 0.09	0.94 ± 0.11	1.02 ± 0.11	2.4%
$B^0 \rightarrow K^{0*} \tau^+ \tau^- [10^{-8}]$	-	6.67 ± 0.87	6.92 ± 0.90	3.7%
$B^0 \rightarrow \rho^0 e^+ e^- [10^{-6}]$	-	1.07 ± 0.18	1.10 ± 0.19	2.4%
$B^0 \rightarrow \rho^0 \mu^+ \mu^- [10^{-7}]$	-	8.9 ± 1.6	9.1 ± 1.7	2.4%
$B^0 \rightarrow \rho^0 \tau^+ \tau^- [10^{-7}]$	-	1.05 ± 0.19	1.09 ± 0.20	3.4%
$B_s^0 \rightarrow \phi e^+ e^- [10^{-6}]$	-	1.52 ± 0.17	1.56 ± 0.17	2.4%
$B_s^0 \rightarrow \phi \mu^+ \mu^- [10^{-6}]$	0.84 ± 0.4	1.15 ± 0.14	1.18 ± 0.15	2.4%
$B_s^0 \rightarrow \phi \tau^+ \tau^- [10^{-8}]$	-	8.11 ± 0.10	8.41 ± 0.11	3.8%
$B_s^0 \rightarrow K^{0*} e^+ e^- [10^{-8}]$	-	5.56 ± 0.65	5.69 ± 0.67	2.4%
$B_s^0 \rightarrow K^{0*} \mu^+ \mu^- [10^{-8}]$	2.9 ± 1.1	4.42 ± 0.56	4.53 ± 0.57	2.4%
$B_s^0 \rightarrow K^{0*} \tau^+ \tau^- [10^{-9}]$	-	4.30 ± 0.50	4.45 ± 0.52	3.5%

TABLE III: Partial decay widths for $B_{d,s}^0 \rightarrow V^0 \ell^+ \ell^-$. Experimental data is taken from [34].

$B_{d,s}^0 \rightarrow V^0 \mu^+ \mu^-$ and $B_{d,s}^0 \rightarrow V^0 e^+ e^-$ differential distributions, the curvature changes from convex to concave for some decay modes (this transition is present in $B^0 \rightarrow \rho^0 \ell^+ \ell^-$ and $B_s^0 \rightarrow K^{0*} \ell^+ \ell^-$, but absent in $B^0 \rightarrow K^{0*} \ell^+ \ell^-$ and $B_s^0 \rightarrow \phi \ell^+ \ell^-$). This change in behavior is almost entirely determined by the energy region $\hat{s} \in (4m_e^2/M_{B_{d,s}^0}^2; 4m_\mu^2/M_{B_{d,s}^0}^2)$. While the muonic decay is kinematically forbidden in this region, the electronic channel still yields a non-zero differential distribution.

In the $B^0 \rightarrow K^{0*} \mu^+ \mu^-$ decay, accounting for Coulomb interaction reduces the discrepancy with experiment from $\delta = 11\%$ to $\delta = 4\%$. For the $B^0 \rightarrow K^{0*} e^+ e^-$ decay, the Coulomb correction increases the discrepancy from $\delta = 14\%$ to $\delta = 17\%$, though the prediction remains within experimental uncertainty. The decays $B_{d,s}^0 \rightarrow V^0 \ell^+ \ell^-$ with τ -leptons demonstrate a Coulomb correction up to $\mathcal{K} = 3.8\%$.

VI. COULOMB INTERACTION IN $B_{d,s}^0 \rightarrow \gamma \ell^+ \ell^-$ DECAYS

In this section, we provide the Coulomb interaction in the decays $B_{d,s}^0 \rightarrow \gamma \ell^+ \ell^-$. The differential decay width is determined similarly to (11) with the pseudoscalar meson h^0 replaced by the photon γ . The explicit expression for $d\Gamma_{B_{s,d}^0 \rightarrow \gamma \ell^+ \ell^-}^{(\text{free})}/d\hat{s}$ is taken from [38].

Differential, angular and double differential distributions are shown on Figs. 9, 10 and 11 in Appendix C.

The partial decay widths for $B_{d,s}^0 \rightarrow \gamma e^+ e^-$ and $B_{d,s}^0 \rightarrow \gamma \mu^+ \mu^-$ are typically calculated within the interval $q^2 \in [1, 6] \text{ GeV}^2$. This choice is motivated by the relatively small contribution from charming loops in this region, which is at the level of a few percent. Consequently, the branching fractions can be predicted with controlled accuracy, limited primarily by the uncertainty in the form factors [38].

In the considered decays, the resonant peaks ρ^0 , ω , J/ψ and $\psi(2S)$ influence on the differential decay width. The J/ψ and $\psi(2S)$ peaks are removed according to the procedure (12), while the ρ^0 and ω fall outside integration region $q^2 \in [1, 6] \text{ GeV}^2$. Predictions for partial widths are presented in Table IV.

To compute decays involving τ -leptons, a different procedure must be employed, as a large part of the interval $q^2 \in [1, 6] \text{ GeV}^2$ is kinematically forbidden. The only resonant peak that needs to be excluded is $\psi(2S)$, which we remove according to (12). The partial width, presented in Table IV, is obtained by integrating over the entire allowed energy range $q^2 \in [4m_\tau^2, M_{B_{d,s}^0}^2]$.

$q^2 \in [1, 6] \text{ GeV}^2$	$\mathcal{B}^{(exp)}$	$\mathcal{B}^{(free)}$	$\mathcal{B}^{(Coulomb)}$	\mathcal{K}
$B_s^0 \rightarrow \gamma e^+ e^- [10^{-9}]$	—	2.97 ± 0.49	3.04 ± 0.50	2.4%
$B_s^0 \rightarrow \gamma \mu^+ \mu^- [10^{-9}]$	< 119 at 90% CL	3.03 ± 0.50	3.10 ± 0.50	2.4%
$B^0 \rightarrow \gamma e^+ e^- [10^{-12}]$	—	5.09 ± 0.59	5.21 ± 0.61	2.3%
$B^0 \rightarrow \gamma \mu^+ \mu^- [10^{-12}]$	—	5.31 ± 0.57	5.43 ± 0.58	2.3%
$q^2 \in [4m_\tau^2, M_{B_{d,s}^0}^2]$	$\mathcal{B}^{(exp)}$	$\mathcal{B}^{(free)}$	$\mathcal{B}^{(Coulomb)}$	\mathcal{K}
$B_s^0 \rightarrow \gamma \tau^+ \tau^- [10^{-9}]$	—	1.13 ± 0.30	1.16 ± 0.31	2.7%
$B^0 \rightarrow \gamma \tau^+ \tau^- [10^{-11}]$	—	3.10 ± 0.93	3.19 ± 0.95	2.7%

TABLE IV: Partial decay widths for $B_{d,s}^0 \rightarrow \gamma \ell^+ \ell^-$ in the interval $q^2 \in [1, 6] \text{ GeV}^2$ for $\ell = \{e, \mu\}$ and $q^2 \in [4m_\tau^2, M_{B_{d,s}^0}^2]$ for $\ell = \tau$. Experimental data is taken from [2].

VII. CONCLUSION

In the present work:

- We have systematically investigated the Coulomb correction in relativistic area. In particular, for scalar particles we considered the non-relativistic Gamow-Sommerfeld-Sakharov (GSS) method and the Crater-Alstine-Sazdjian (CAS) approach of exact relativistic two-particle equations. Using CAS equations, we derived the Coulomb correction (3), see Appendix B. A comparison with 1-loop QED calculations [31] has also been performed. Based on the conducted analysis, we conclude that to account for the Coulomb interaction between final

state charged leptons in the decays of neutral B -mesons, it is sufficient to use either correction (2) or (3) with the relativistic relative velocity.

- The Coulomb correction has been obtained for:
 - Ultra-rare leptonic decays $B_{d,s}^0 \rightarrow \ell^+ \ell^-$, see Table I;
 - Rare semileptonic decays $B^0 \rightarrow \{K^0, \pi^0\} \ell^+ \ell^-$ and $B_s^0 \rightarrow \{\eta, \eta', K^0\} \ell^+ \ell^-$ involving pseudoscalar mesons, see Table II, Figs. 2, 3, 4, 5;
 - Rare semileptonic decays $B^0 \rightarrow \{K^{0*}, \rho^0\} \ell^+ \ell^-$ and $B_s^0 \rightarrow \{\phi, K^{0*}\} \ell^+ \ell^-$ involving vector mesons, see Table III, Figs. 6, 7, 8;
 - Rare radiative leptonic decays $B^0 \rightarrow \gamma \ell^+ \ell^-$, see Table IV, Figs. 9, 10, 11.
- The following key results have been obtained:
 - Accounting for the Coulomb interaction in the decay $B_s^0 \rightarrow \mu^+ \mu^-$ reduces the discrepancy between the average experimental value and the theoretical prediction within the SM to $\delta = 2\%$. However, this improvement is small compared to the current experimental (11% [13]) and theoretical (5% [32]) uncertainties for the partial width of this decay.
 - In the decay $B^0 \rightarrow K^{0*} \mu^+ \mu^-$, the correction reduces the discrepancy between theoretical predictions and experimental data from $\delta = 11\%$ to $\delta = 4\%$, against the background of an 8% experimental error [34].
 - In the decay $B^0 \rightarrow K^{0*} e^+ e^-$, the Coulomb correction increases the discrepancy between theoretical predictions and experimental data from $\delta = 14\%$ to $\delta = 17\%$, yet remains within the experimental uncertainty (17%, [34]).
 - In the decay $B^0 \rightarrow K^0 \mu^+ \mu^-$, the correction reduces the discrepancy between theoretical predictions and experimental data from $\delta = 1.7\%$ to $\delta = 0.5\%$, against the background of a 10% experimental error [34].
 - In decays with τ -leptons in the final state (particularly in $B_s^0 \rightarrow \eta' \tau^+ \tau^-$ and $B_s^0 \rightarrow \phi \tau^+ \tau^-$), the correction reaches $\mathcal{K} \sim 4\%$. This correction is currently smaller than both dominant form-factor uncertainties and experimental errors; however, it represents a meaningful systematic effect that must be accounted for in future high-precision experimental analyses.

The obtained results demonstrate that accounting for Coulomb corrections is an essential element of the theoretical analysis of rare leptonic and semileptonic decays of neutral B -mesons. In particular, for decays with electrons and muons, the corrections (2-3%), although

smaller than the current experimental uncertainties (5–15% [34]), improve the accuracy of predictions. For channels with τ -leptons, the corrections reach 4%. This suggests that the discussed correction may become significant for future high-precision experiments in B -physics, especially those involving τ -leptons in the final states.

VIII. FUNDING

For one of the authors, N.V. Nikitin, this work was supported by Russian Science Foundation (grant no. 25-

22-00614 rare fourlepton decays of heavy mesons in the orthogonal amplitude technique)

IX. CONFLICT OF INTEREST

The authors of this work declare that they have no conflicts of interest.

[1] R. Aaij et al. (LHCb), *JHEP* **09**, 026 (2024).
[2] R. Aaij et al. (LHCb), *JHEP* **07**, 101 (2024).
[3] R. Aaij et al. (LHCb), *Phys. Rev. Lett.* **131**, 051803 (2023).
[4] R. Aaij et al. (LHCb), *Nature Phys.* **18**, 277 (2022).
[5] R. Aaij et al. (LHCb), *Phys. Rev. Lett.* **128**, 041801 (2022).
[6] R. Aaij et al. (LHCb), *Phys. Rev. D* **105**, 012010 (2022).
[7] R. Aaij et al. (LHCb), *Phys. Rev. Lett.* **118**, 191801 (2017).
[8] R. Aaij et al. (LHCb), *JHEP* **04**, 142 (2017).
[9] R. Aaij et al. (LHCb), *JHEP* **06**, 133 (2014).
[10] R. Aaij et al. (LHCb), *Phys. Rev. Lett.* **127**, 151801 (2021), 2105.14007.
[11] A. Hayrapetyan et al. (CMS), *Phys. Lett. B* **864**, 139406 (2025).
[12] A. Hayrapetyan et al. (CMS), *Rept. Prog. Phys.* **87**, 077802 (2024).
[13] A. Tumasyan et al. (CMS), *Phys. Lett. B* **842**, 137955 (2023).
[14] M. Aaboud et al. (ATLAS), *JHEP* **04**, 098 (2019).
[15] I. Adachi et al. (Belle and Belle-II), *Phys. Rev. Lett.* **133**, 101804 (2024).
[16] L. Aggarwal et al. (Belle-II), *Phys. Rev. Lett.* **131**, 051804 (2023).
[17] F. Abudin et al. (Belle-II) (2022), 2206.05946.
[18] A. J. Buras, *Nucl. Instrum. Meth. A* **368**, 1 (1995).
[19] G. Buchalla, A. J. Buras, and M. E. Lautenbacher, *Rev. Mod. Phys.* **68**, 1125 (1996).
[20] A. J. Buras, *Subnucl. Ser.* **38**, 200 (2002), hep-ph/0101336.
[21] M. Beneke, C. Bobeth, and R. Szafron, *JHEP* **10**, 232 (2019).
[22] D. Melikhov, N. Nikitin, and S. Simula, *Phys. Rev. D* **57**, 6814 (1998).
[23] D. Melikhov and N. Nikitin, *Phys. Rev. D* **70**, 114028 (2004).
[24] A. Danilina, N. Nikitin, and K. Toms, *Phys. Rev. D* **101**, 096007 (2020).
[25] G. Gamow, *Zeitschrift für Physik* **51**, 204 (1928).
[26] A. Sommerfeld, *Atombau und Spektrallinien* (F. Vieweg & Sohn, 1921).
[27] A. D. Sakharov, *Sov. Phys. Usp.* **34**, 375–377 (1991).
[28] H. W. Crater and P. V. Alstine, *Annals Phys.* **148**, 57 (1983).
[29] H. W. Crater and P. V. Alstine, *Found. Phys.* **24**, 297 (1994).
[30] H. Sazdjian, *Phys. Rev. D* **33**, 3401 (1986).
[31] A. Arbuzov and T. Kopylova, *Journal of High Energy Physics* **2012** (2011).
[32] Y. Aoki et al. (Flavour Lattice Averaging Group (FLAG)) (2024), 2411.04268.
[33] A. J. Buras and M. Münz, *Phys. Rev. D* **52**, 186 (1995).
[34] S. Navas et al. (Particle Data Group), *Phys. Rev. D* **110**, 030001 (2024).
[35] D. Melikhov, N. Nikitin, and S. Simula, *Phys. Lett. B* **430**, 332 (1998).
[36] D. Melikhov and B. Stech, *Phys. Rev. D* **62**, 014006 (2000).
[37] N. Gubernari, A. Kokulu, and D. van Dyk, *JHEP* **01**, 150 (2019).
[38] A. Kozachuk, D. Melikhov, and N. Nikitin, *Phys. Rev. D* **97**, 053007 (2018), 1712.07926.
[39] I. T. Todorov, *Phys. Rev. D* **3**, 2351 (1971).
[40] W. Greiner (Springer-Verlag, New York, 2000).

Appendix A: Relativistic two-particle equations

This appendix outlines the relativistic two-particle formalism developed by Crater, Alstine, and Sazdjian (CAS)[28–30] based on relativistic classical constrained dynamics with the following quantisation. The CAS approach provides a rigorous, fully relativistic description of two-body interactions. Since the original derivation is rather involved we present here a condensed version of the formalism, focusing only on the essential steps required to derive the relativistic Coulomb factor used in our analysis.

Let us consider a system of two interacting scalar particles. In most general form the equations these scalar particles must obey can be written as follows:

$$\mathcal{H}_1|\psi\rangle = (p_1^2 - m_1^2 - \Phi_1) |\psi\rangle = 0 \quad (A1)$$

$$\mathcal{H}_2|\psi\rangle = (p_2^2 - m_2^2 - \Phi_2) |\psi\rangle = 0 \quad (A2)$$

where $p_i^2 = p_i^\mu p_{i\mu}$ is the squared momentum operator of the i -th particle, m_i is the mass of the i -th particle, and Φ_i is the interaction operator.

The key condition (or constraint) for these equations is the requirement $[\mathcal{H}_1, \mathcal{H}_2]|\psi\rangle = 0$. In the simplest case, this can be achieved when:

$$\Phi_1 = \Phi_2 \equiv \Phi(x_\perp) \quad (\text{A3})$$

where $x_\perp^\mu = x^\mu - (x \cdot P)P^\mu/P^2$ is the transverse relative coordinate orthogonal to the total 4-momentum of the system $P^\mu = p_1^\mu + p_2^\mu = (E, \mathbf{P})$. Equation (A3) can be regarded as a relativistic generalization of Newton's third law.

We introduce the center of mass energy variables:

$$\epsilon_1 = \frac{P^2 + m_1^2 - m_2^2}{2\sqrt{P^2}}, \quad \epsilon_2 = \frac{P^2 + m_2^2 - m_1^2}{2\sqrt{P^2}} \quad (\text{A4})$$

and the relative 4-momentum q^μ :

$$p_1^\mu = \frac{\epsilon_1}{\sqrt{P^2}} P^\mu + q^\mu, \quad p_2^\mu = \frac{\epsilon_2}{\sqrt{P^2}} P^\mu - q^\mu \quad (\text{A5})$$

Then the equation of motion takes the form:

$$\begin{aligned} \mathcal{H}|\psi\rangle &= \mathcal{H}_1|\psi\rangle = \mathcal{H}_2|\psi\rangle = \\ &(\epsilon_1^2 - m_1^2 + q^2 - \Phi(x_\perp))|\psi\rangle = \\ &(\epsilon_2^2 - m_2^2 + q^2 - \Phi(x_\perp))|\psi\rangle = \\ &(b^2(P^2, m_1^2, m_2^2) + q^2 - \Phi(x_\perp))|\psi\rangle = 0, \end{aligned} \quad (\text{A6})$$

where the relativistic invariant b^2 is defined as

$$\begin{aligned} b^2(P^2, m_1^2, m_2^2) &= \epsilon_1^2 - m_1^2 = \epsilon_2^2 - m_2^2 = \\ &= \frac{1}{4P^2}(P^4 - 2P^2(m_1^2 + m_2^2) + (m_1^2 - m_2^2)^2) \end{aligned} \quad (\text{A7})$$

Using Todorov's kinematic variables [39]:

$$m_s = \frac{m_1 m_2}{\sqrt{s}}, \quad \epsilon_s = \frac{s - m_1^2 - m_2^2}{2\sqrt{s}}, \quad s \equiv P^2 \quad (\text{A8})$$

and an auxiliary momentum:

$$\mathcal{P}^\mu = q^\mu + \epsilon_s \frac{P^\mu}{\sqrt{s}} \quad (\text{A9})$$

the equation takes the form:

$$\begin{aligned} (b^2(s^2, m_1^2, m_2^2) + q^2 - \Phi(x_\perp))|\psi\rangle &= \\ &= (\epsilon_s^2 - m_s^2 + q^2 - \Phi(x_\perp))|\psi\rangle = \\ &= (\mathcal{P}^2 - m_s^2 - \Phi(x_\perp))|\psi\rangle = 0 \end{aligned} \quad (\text{A10})$$

This is the equation of relative motion for scalar particles in its most general form. Next, we need to specify

the form of the interaction potential $\Phi(x_\perp)$. We are interested in the Coulomb interaction, which can be derived using the standard procedure:

$$\mathcal{P}^\mu \rightarrow \mathcal{P}^\mu - A^\mu, \quad A^\mu = (U(r), \mathbf{0}) = (-\alpha_{\text{em}}/r, \mathbf{0}) \quad (\text{A11})$$

which leads to the final equation in the center of mass system ($\mathbf{P} = 0$):

$$[(\epsilon_s - U(r))^2 - \mathbf{q}^2 - m_s^2] \psi(\mathbf{r}) = 0 \quad (\text{A12})$$

where $\mathbf{q}^2 \equiv -\nabla^2$.

Appendix B: Derivation of the Coulomb correction within the CAS approach.

This appendix presents the derivation of the Coulomb correction factor (3) within the CAS approach for the scalar decay $B^0 \rightarrow S^+ S^-$. We begin by solving the CAS equation for the relative motion of the charged scalar $S^+ S^-$ -pair in the s-wave ($l = 0$) state. The obtained solution exhibits a weak divergence at the origin. We analyze this divergence, show that it lies outside the domain of validity of the CAS approximation, and estimate the range of particle velocities where its contribution is negligible. This allows us to arrive at the final expression for the correction factor.

To solve the CAS equation (A12), we separate the variables in the wave function, $\psi^{(\text{Coulomb})}(\mathbf{r}) = R_{nl}(r)Y_{lm}(\theta, \phi)$, which yields the equation for the radial component:

$$\left(\frac{d^2}{dz^2} + \frac{2}{z} \frac{d}{dz} - \frac{l(l+1)}{z^2} + \frac{2\eta}{z} + \frac{\alpha_{\text{em}}^2}{z^2} + 1 \right) R_{nl}(r) = 0 \quad (\text{B1})$$

where $z = pr$, $p = \sqrt{\epsilon_s^2 - m_s^2}$, $\eta = \alpha_{\text{em}}/v$, $v = p/\epsilon_s$.

Note that the velocity v in this case coincides with the relative velocity:

$$v = \frac{\sqrt{\epsilon_s^2 - m_s^2}}{m_s} = \frac{\sqrt{s^2 - 4m^2s}}{s - 2m^2} = v_{\text{rel}} \quad (\text{B2})$$

The positive-frequency solution of equation (B1) is [40]:

$$R_{nl}^{(+)}(r) = \frac{|\Gamma(a)|}{\Gamma(b)} e^{\pi\eta/2} \cdot (2ipr)^{\mu - \frac{1}{2}} e^{ipr} F(a, b, -2ipr) \quad (\text{B3})$$

$$a = \mu + \frac{1}{2} + i\eta, \quad b = 2\mu + 1; \quad \mu = \sqrt{\left(l + \frac{1}{2}\right)^2 - \alpha_{\text{em}}^2} \quad (\text{B4})$$

where $\Gamma(z)$ is Euler's gamma function, and $F(a, b, z)$ is Kummer's confluent hypergeometric function.

The Coulomb correction is typically computed as the ratio $|\psi^{(\text{Coulomb})}(0)|^2/|\psi^{(\text{free})}(0)|^2 = |\psi^{(\text{Coulomb})}(0)|^2$, where we have used that $|\psi^{(\text{free})}(\mathbf{r})|^2 = |e^{i\mathbf{p}\mathbf{r}}|^2 = 1$. It is important to note that in this standard approach, the wave function is evaluated not at the strict mathematical origin, but at a “physical zero”—a distance much smaller than any typical scale of the problem and within the domain of validity of the underlying equations.

In our case, the decay $B \rightarrow S^+ S^-$ has zero orbital angular momentum ($l = 0$), and therefore the wave function exhibits a weak divergence at $r \rightarrow 0$, associated with the factor $(2ipr)^{\mu-1/2}$. This divergence is removed by evaluating the wave function at a point shifted by a small distance R from the center. Such a regularization is possible because the derivation of the CAS equations assumed a constant electromagnetic coupling, $\alpha_{\text{em}}(r) \approx \alpha_{\text{em}} \approx 1/137$, which is valid only at distances larger than the Compton wavelength, $R \gg 1/m$. Consequently, the solutions of the CAS equation are physically reliable only on the scale $r \gtrsim 1/m$.

To quantify when this regularization is negligible, we examine the factor $(2ipr)^{\mu-1/2}$ at the scale $\varkappa \equiv pR \ll 1$. Expanding its squared modulus yields:

$$\begin{aligned} |(2i\varkappa)^{\mu-1/2}|^2 &= (2\varkappa)^2 \sqrt{1/4 - \alpha_{\text{em}}^2} - 1 = e^{-2\alpha_{\text{em}}^2 \ln(2\varkappa) + O(\alpha_{\text{em}}^4)} \\ &= 1 - 2\alpha_{\text{em}}^2 \ln(2\varkappa) + O(\alpha_{\text{em}}^4 \ln^2(\varkappa)). \end{aligned} \quad (\text{B5})$$

This factor can be treated as constant (≈ 1) provided $-2\alpha_{\text{em}}^2 \ln(2\varkappa) \ll 1$. Using (B2) for the relative velocity v and the condition $R \sim 1/m$, we find the resulting constraint on the velocity of the $S^+ S^-$ pair:

$$\sqrt{1 - 4m^2/s} \gg e^{-1/(2\alpha_{\text{em}}^2)} \approx 10^{-4000}.$$

This inequality is satisfied for any physically relevant velocity.

Therefore, the weak divergence at the origin can be safely ignored. The CAS factor is obtained by evaluating the wave function in Eq. (B3) at $r = 0$, discarding the divergent factor $(2ipr)^{\mu-1/2}$ (which is set to unity as shown above), and using $F(a, b, 0) = 1$. The final, regularized result is:

$$\begin{aligned} \mathcal{K}^{(CS)} &= \left| \frac{\Gamma(a)}{\Gamma(b)} \cdot e^{\pi\alpha_{\text{em}}/(2v)} \right|^2 = \left| \frac{\Gamma(a)}{\Gamma(b)} \right|^2 \cdot e^{\pi\alpha_{\text{em}}/v} \\ &= \left| \frac{\Gamma\left(\sqrt{\frac{1}{4} - \alpha_{\text{em}}^2} + \frac{1}{2} + i\frac{\alpha_{\text{em}}}{v}\right)}{\Gamma\left(\sqrt{1 - 4\alpha_{\text{em}}^2} + 1\right)} \right|^2 \cdot e^{\pi\alpha_{\text{em}}/v}. \end{aligned} \quad (\text{B6})$$

Appendix C: Differential, angle and double differential distributions

This appendix contains the complete set of differential, angular, and double differential distributions for all decay channels studied in this work. The figures are organized as follows:

- Fig. 3: Differential distributions $d\mathcal{B}/d\hat{s}$ for decays with pseudoscalar mesons $B_{d,s}^0 \rightarrow h^0 \ell^+ \ell^-$.
- Fig. 4: Angular distributions $d\mathcal{B}/d\cos\theta$ for the same pseudoscalar channels.
- Fig. 5: Double differential distributions $d\mathcal{B}/d\hat{s}d\cos\theta$ for pseudoscalar meson decays.
- Fig. 6: Differential distributions $d\mathcal{B}/d\hat{s}$ for decays with vector mesons $B_{d,s}^0 \rightarrow V^0 \ell^+ \ell^-$.
- Fig. 7: Angular distributions $d\mathcal{B}/d\cos\theta$ for vector meson channels.
- Fig. 8: Double differential distributions $d\mathcal{B}/d\hat{s}d\cos\theta$ for vector meson decays.
- Fig. 9: Differential distributions $d\mathcal{B}/d\hat{s}$ for radiative leptonic decays $B_{d,s}^0 \rightarrow \gamma \ell^+ \ell^-$.
- Fig. 10: Angular distributions $d\mathcal{B}/d\cos\theta$ for radiative leptonic decays.
- Fig. 11: Double differential distributions $d\mathcal{B}/d\hat{s}d\cos\theta$ for radiative leptonic decays.

Here $\hat{s} = (p_{B_{d,s}^0} - p_X)^2/M_{B_{d,s}^0}^2$ denotes the squared transferred four-momentum normalized to the square of the $B_{d,s}^0$ -meson mass, where X stands for the corresponding final-state particle (h^0 , V^0 or γ) and the angular variable $\cos\theta$ is defined via the angle θ between the momentum of the particle X and the momentum of the positive lepton ℓ^+ in the dilepton ($\ell^+ \ell^-$) rest frame.

In all plots, the black band represents theoretical predictions without Coulomb interaction, the gray band includes Coulomb corrections, and the overlapping region is shown with black-gray hatching.

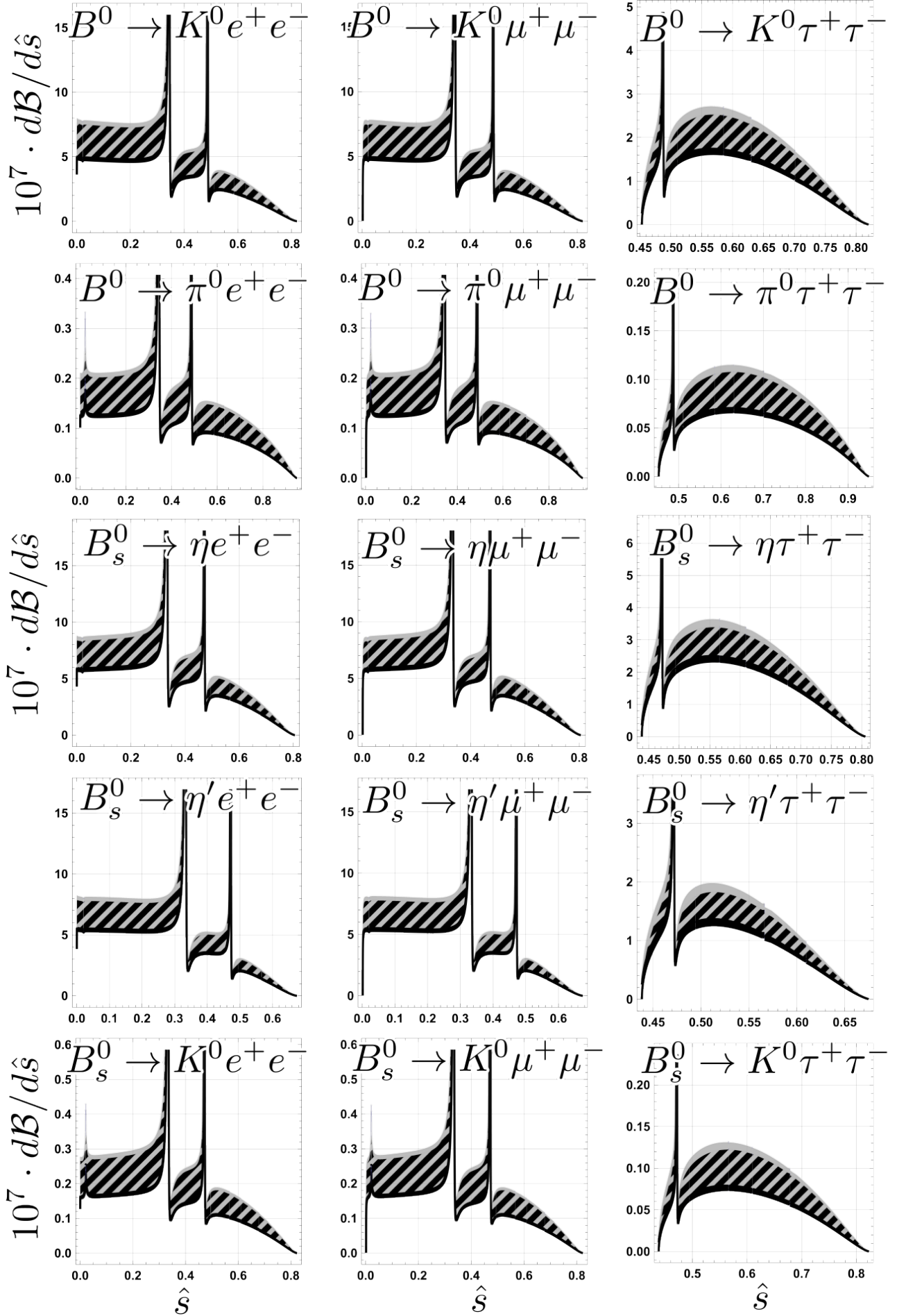


FIG. 3: Dependence of the differential branching fraction $10^7 d\mathcal{B}/d\hat{s}$ for the decays $B^0 \rightarrow \{K^0, \pi^0\} \ell^+ \ell^-$ and $B_s^0 \rightarrow \{\eta, \eta', K^0\} \ell^+ \ell^-$ on $\hat{s} = (p_{B_{d,s}^0} - p_{h^0})^2/M_{B_{d,s}^0}^2$ — the squared transferred momentum normalized to the square of the B -meson mass. The black band corresponds to predictions without Coulomb interaction, the gray band — with Coulomb interaction. The overlap region is indicated by black-gray hatching.

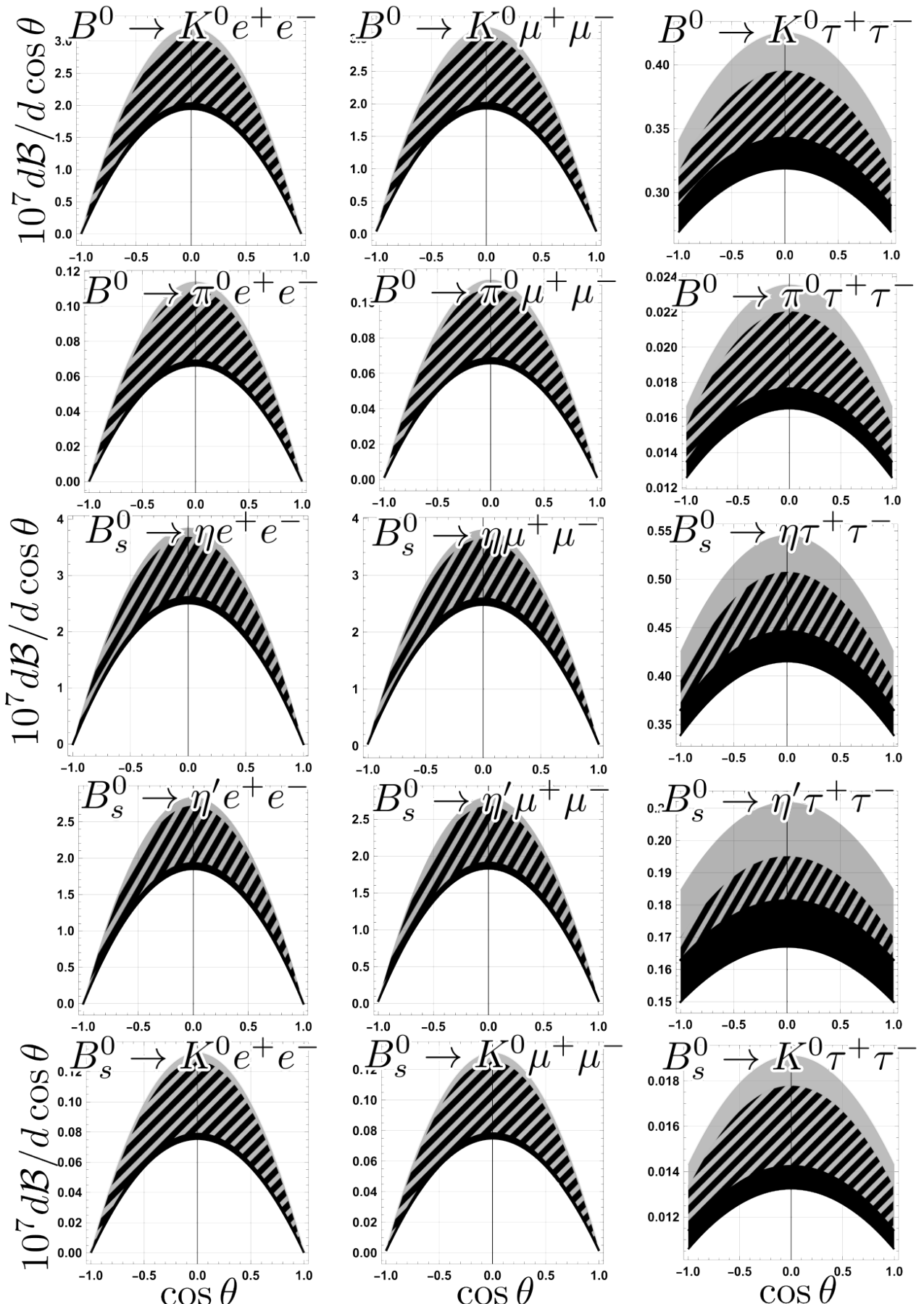


FIG. 4: Angular distributions $10^7 d\mathcal{B}/d \cos \theta$ for the decays $B^0 \rightarrow \{K^0, \pi^0\} \ell^+ \ell^-$ and $B_s^0 \rightarrow \{\eta, \eta', K^0\} \ell^+ \ell^-$ as a function of $\cos \theta$, where $\theta = \angle(\mathbf{p}_{h^0}, \mathbf{p}_{\ell^+})$ is the angle between the direction of the neutral hadron h^0 and the positive lepton ℓ^+ in the $\ell^+ \ell^-$ rest frame. The black band corresponds to predictions without Coulomb interaction, the gray band — with Coulomb interaction. The overlap region is indicated by black-gray hatching.

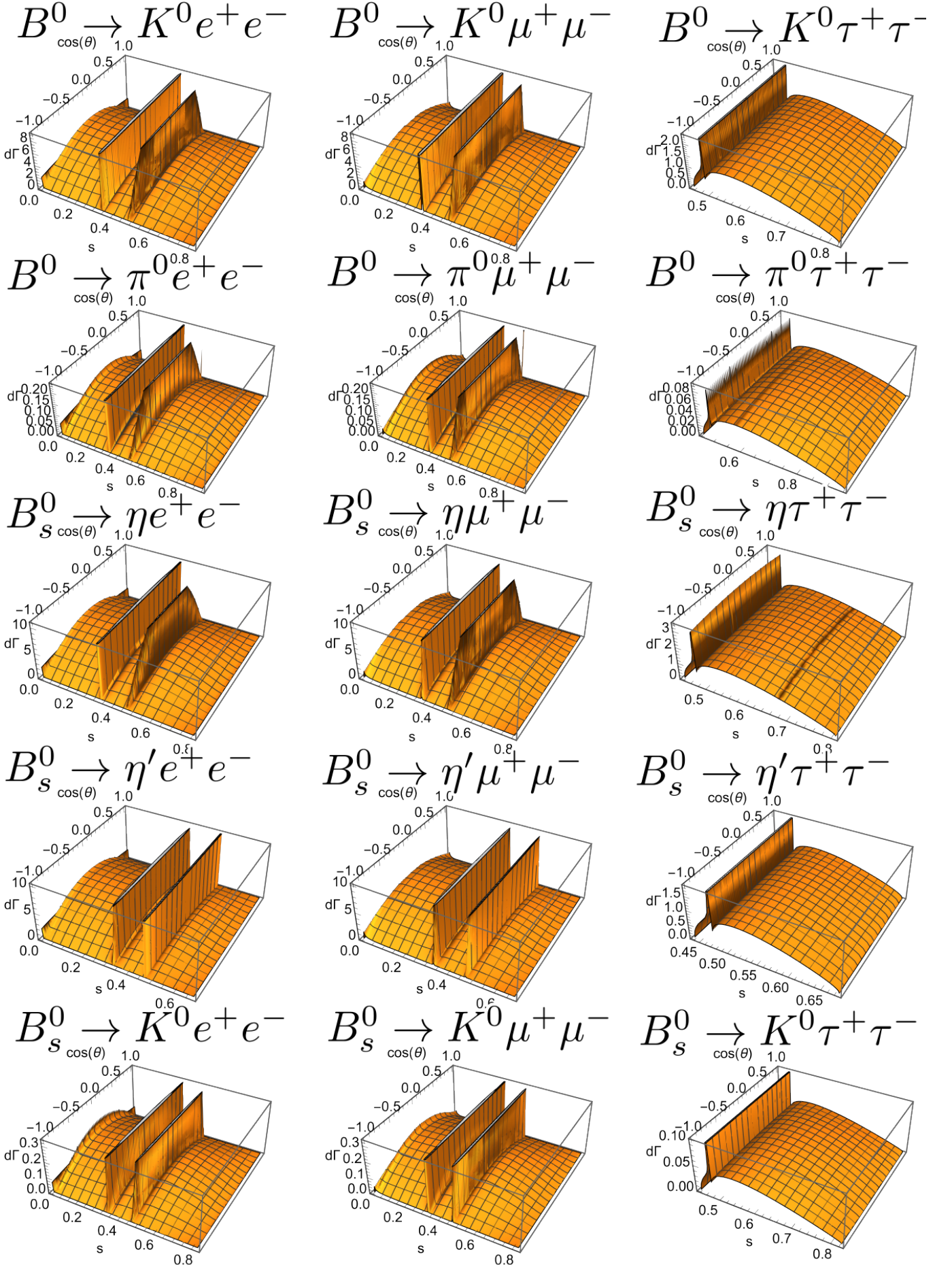


FIG. 5: Double differential distributions $10^7 \cdot d\mathcal{B}/d\hat{s} d\cos\theta$ for the decays $B^0 \rightarrow \{K^0, \pi^0\} \ell^+ \ell^-$ and $B_s^0 \rightarrow \{\eta, \eta', K^0\} \ell^+ \ell^-$. Here $\hat{s} = (p_{B_{d,s}^0} - p_{h^0})^2/M_{B_{d,s}^0}^2$ and $\theta = \angle(\mathbf{p}_{h^0}, \mathbf{p}_{\ell^+})$ is the angle between the direction of the neutral hadron h^0 and the positive lepton ℓ^+ in the $\ell^+ \ell^-$ rest frame.

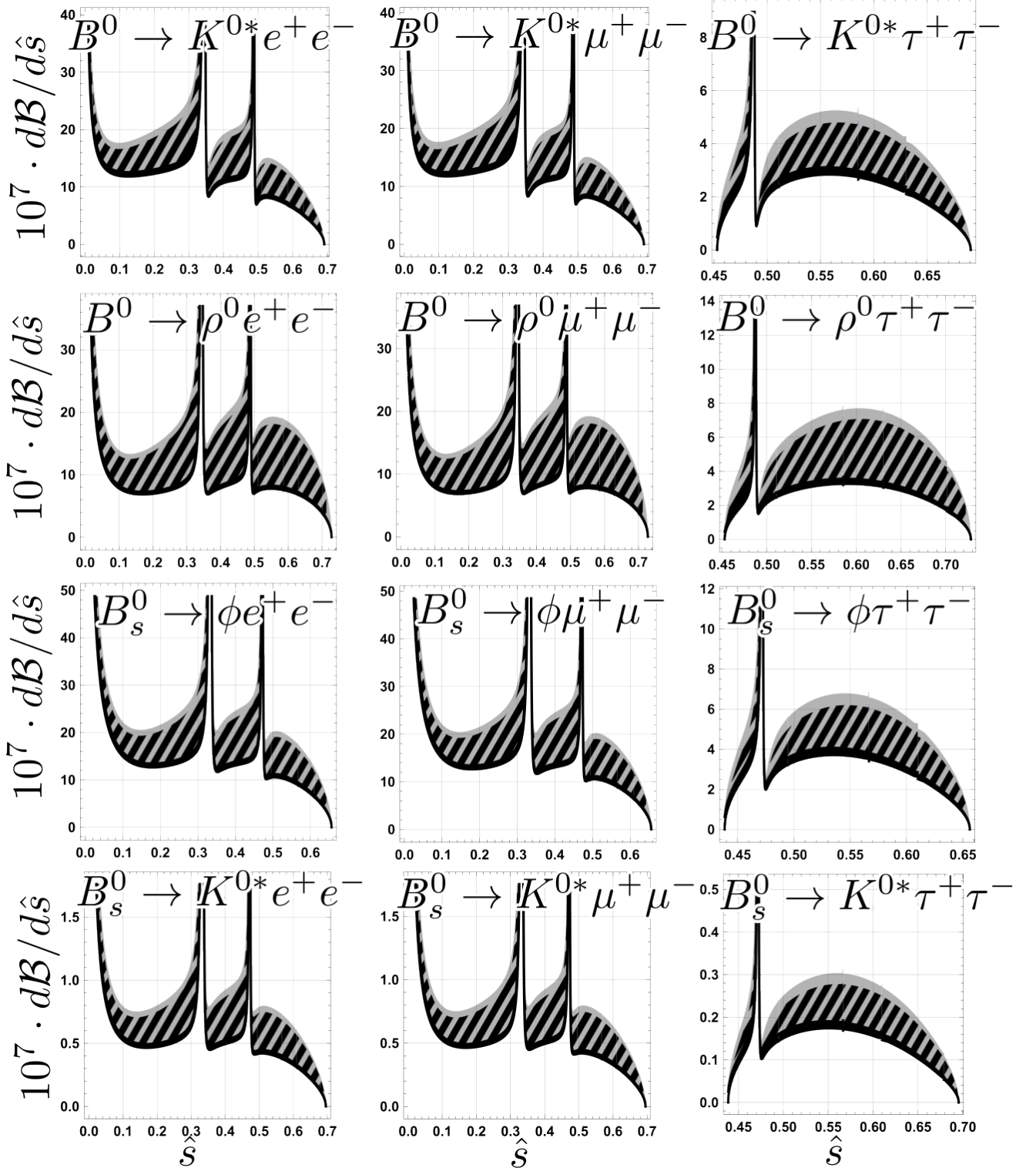


FIG. 6: Dependence of the differential branching fraction $10^7 d\mathcal{B}/d\hat{s}$ for the decays $B^0 \rightarrow \{K^{0*}, \rho^0\} \ell^+ \ell^-$ and $B_s^0 \rightarrow \{\phi, K^{0*}\} \ell^+ \ell^-$ on $\hat{s} = (p_{B_{d,s}^0} - p_{V^0})^2/M_{B_{d,s}^0}^2$ — the squared transferred momentum normalized to the square of the B -meson mass. The black band corresponds to predictions without Coulomb interaction, the gray band — with Coulomb interaction. The overlap region is indicated by black-gray hatching.

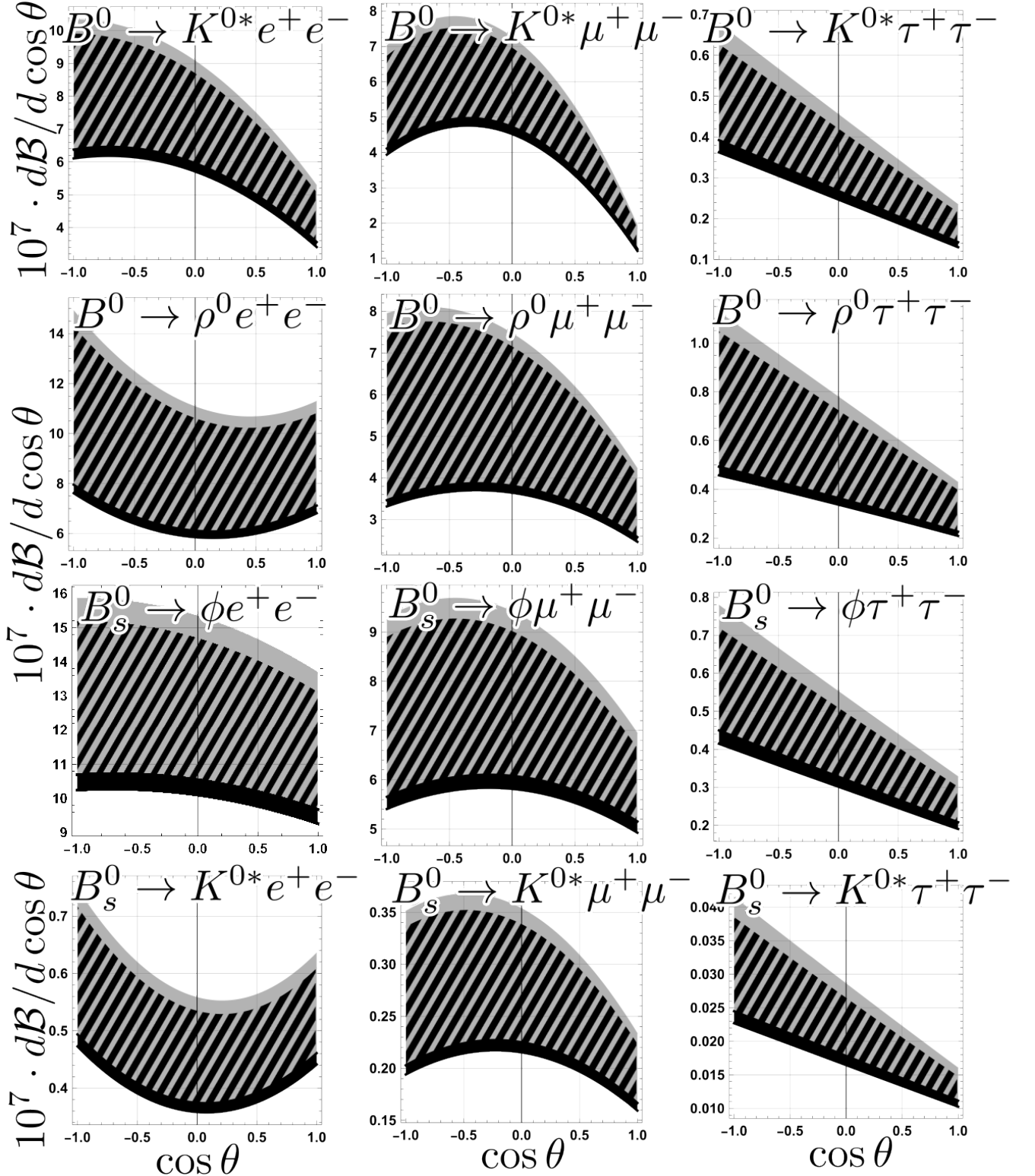


FIG. 7: Angular distributions for $B^0 \rightarrow \{K^{0*}, \rho^0\} \ell^+ \ell^-$ and $B_s^0 \rightarrow \{\phi, K^{0*}\} \ell^+ \ell^-$ as a function of $\cos \theta$, where $\theta = \angle(\mathbf{p}_{V^0}, \mathbf{p}_{\ell^+})$ is the angle between the direction of the neutral hadron V^0 and the positive lepton ℓ^+ in the $\ell^+ \ell^-$ rest frame. The black band corresponds to predictions without Coulomb interaction, the gray band — with Coulomb interaction. The overlap region is indicated by black-gray hatching.

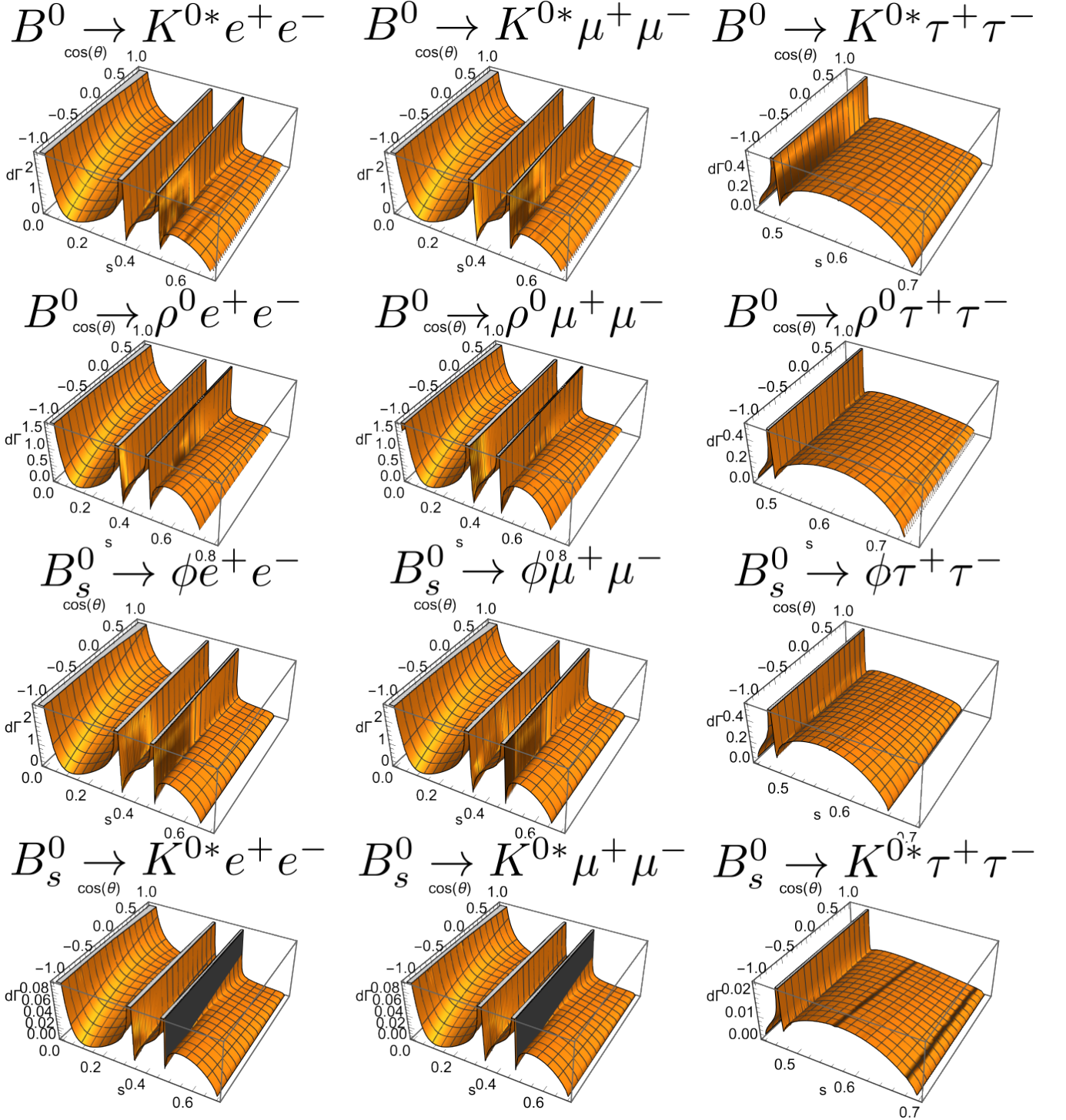


FIG. 8: Double differential distributions $10^7 \cdot d\mathcal{B}/d\hat{s}d\cos\theta$ for $B^0 \rightarrow \{K^{0*}, \rho^0\}\ell^+\ell^-$ and $B_s^0 \rightarrow \{\phi, K^{0*}\}\ell^+\ell^-$. Here $\hat{s} = (p_{B_{d,s}^0} - p_{V^0})^2/M_{B_{d,s}^0}^2$ and $\theta = \angle(\mathbf{p}_{V^0}, \mathbf{p}_{\ell^+})$ is the angle between the direction of the neutral hadron V^0 and the positive lepton ℓ^+ in the $\ell^+\ell^-$ rest frame.

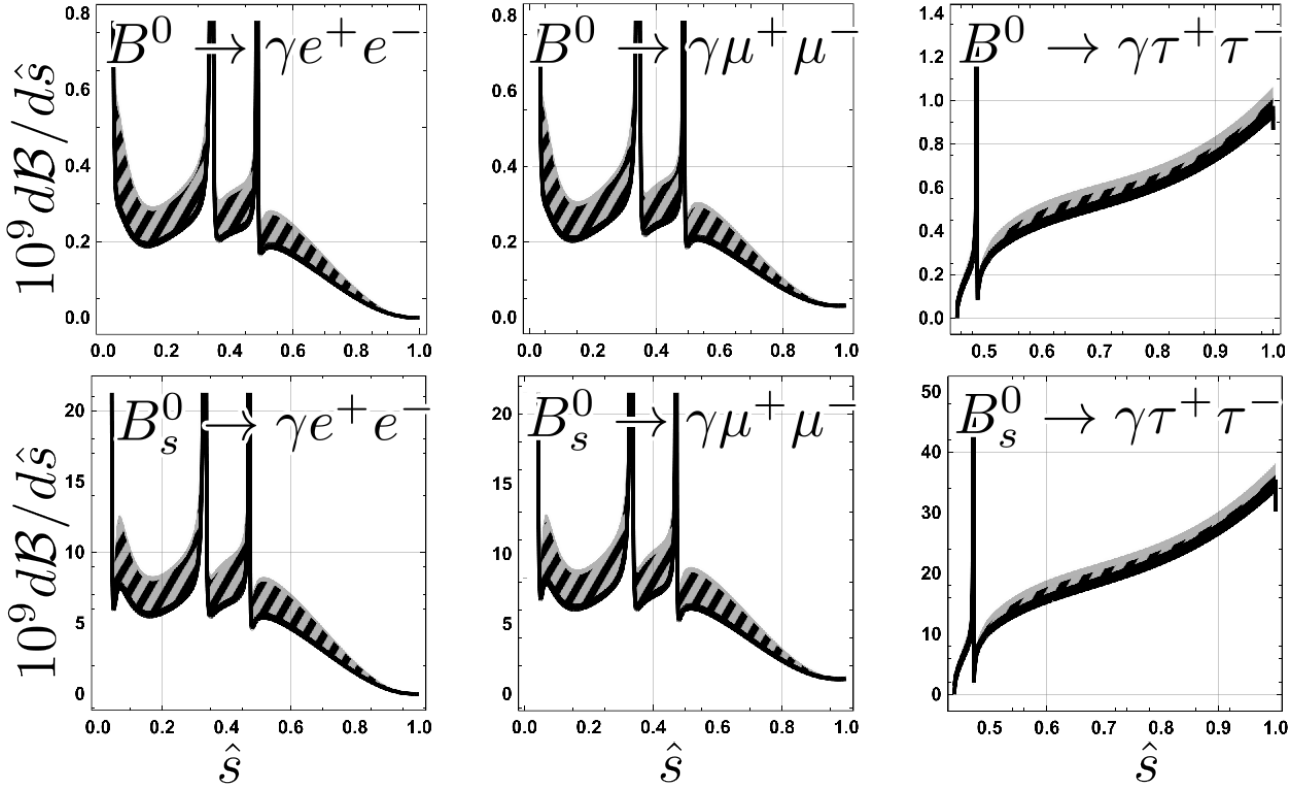


FIG. 9: Dependence of the differential branching fraction $10^9 d\mathcal{B}/d\hat{s}$ for the decays $B_{d,s}^0 \rightarrow \gamma \ell^+ \ell^-$ on $\hat{s} = (p_{B_{d,s}^0} - p_\gamma)^2/M_{B_{d,s}^0}^2$. The black band corresponds to predictions without Coulomb interaction, the gray band — with Coulomb interaction. The overlap region is indicated by black-gray hatching.

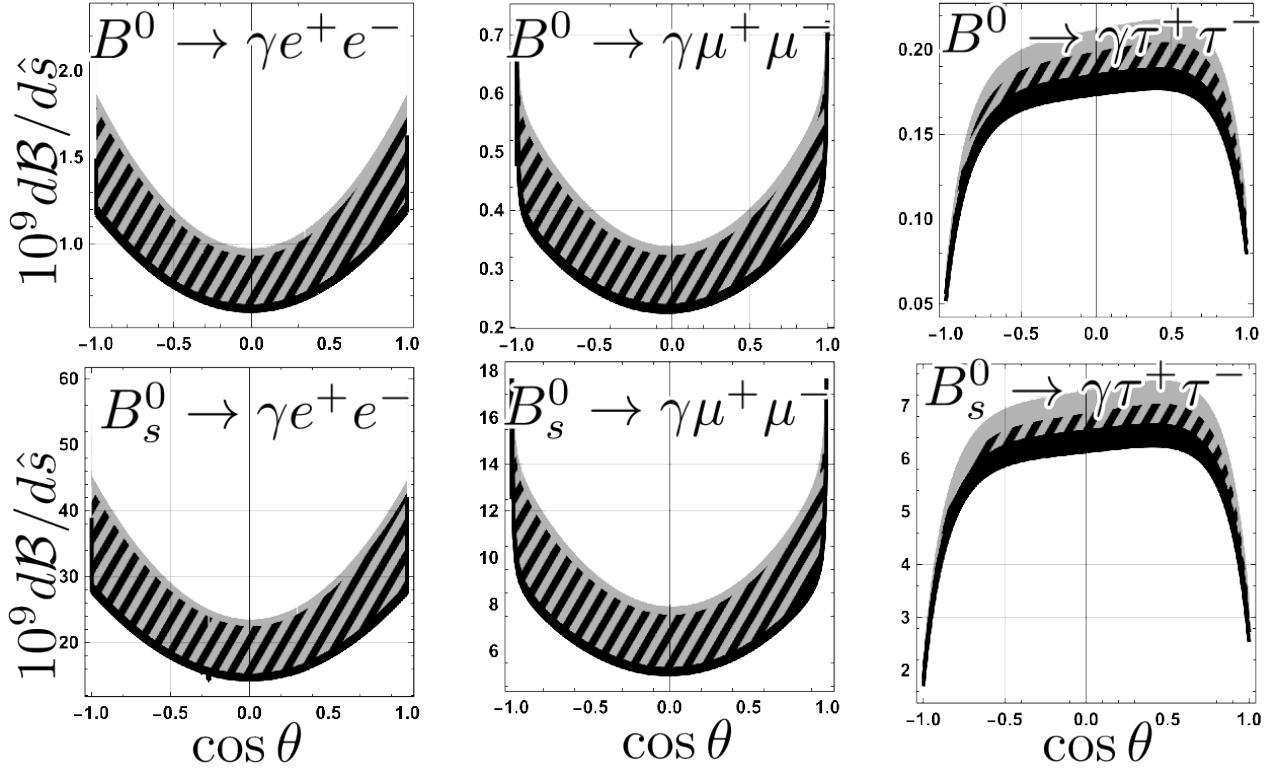


FIG. 10: Angular distributions for $B_{d,s}^0 \rightarrow \gamma \ell^+ \ell^-$ as a function of $\cos \theta$, where $\theta = \angle(\mathbf{p}_\gamma, \mathbf{p}_{\ell^+})$ is the angle between the direction of the photon γ and the positive lepton ℓ^+ in the $\ell^+ \ell^-$ rest frame. The black band corresponds to predictions without Coulomb interaction, the gray band — with Coulomb interaction. The overlap region is indicated by black-gray hatching.

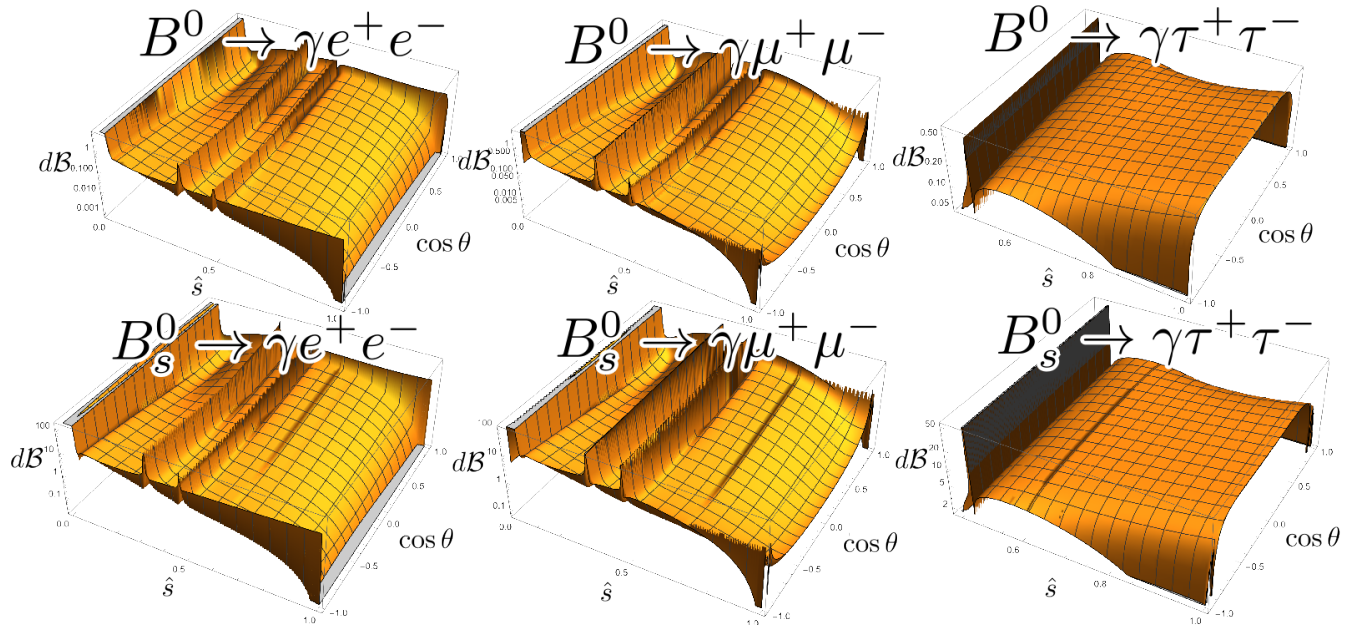


FIG. 11: Double differential distributions $10^9 \cdot d\mathcal{B}/d\hat{s} d\cos \theta$ for $B_{d,s}^0 \rightarrow \gamma \ell^+ \ell^-$. Here $\hat{s} = (p_{B_{d,s}^0} - p_\gamma)^2/M_{B_{d,s}^0}^2$ and $\theta = \angle(\mathbf{p}_\gamma, \mathbf{p}_{\ell^+})$ is the angle between the direction of the photon γ and the positive lepton ℓ^+ in the $\ell^+ \ell^-$ rest frame.